

# **Image-Based Control of Skin Melanin Texture**

**Norimichi Tsumura\*\*\*, Toshiya Nakaguchi\*, Nobutoshi Ojima\*\*\*,  
Koichi Takase\*, Saya Okaguchi\*, Kimihiko Hori\*\*\*, Yoichi Miyake\***

\*Department of Information and Image Sciences, Chiba University

1-33 Yayoi-cho, Inage-ku, Chiba 263-8522, JAPAN

\*\*PRESTO, Japan Science and Technology Agency

Kawaguchi Center Building, 4-1-8, Honcho, Kawaguchi-shi, Saitama, 332-0012, JAPAN

\*\*\*Kao Corporation

2-1-3 Bunka, Sumida-ku, Tokyo, 131-8501, JAPAN

## Abstract

This paper introduces a useful tool for controlling the skin melanin texture of facial photographs. Controlling the skin melanin texture is an important task in the reproduction of posters, TV commercials, movies, and so on. We used component maps of melanin, which were obtained by our previous method [JOSA A, Vol. 16 No. 9, 2169-2176(1999)] as the first step of processing. We propose to control the melanin texture continuously and physiologically, based on the analysis of 123 skin textures in our database. The physiological validity for the change of the melanin texture is confirmed by comparing the synthesized image with an ultraviolet image, which can predict the change of melanin texture due to aging. The control processes are implemented on programmable graphics hardware, and real-time processing is achieved for a facial video stream.

*OCIS codes:* 100.2960, 100.2980, 110.7050

## 1. Introduction

The appearance of human skin is an essential attribute in computer graphics. Skin appearance is mainly caused by the texture of the skin, and people are very sensitive to any change of the skin appearance in photographs and other reproduced images. Since the modeling and rendering of realistic human skin in computer graphics requires much time and effort, a photograph of a human face is often used as the basic element. In the reproduction of human images in posters, TV commercials, movies and other media, the skin melanin texture of the photograph is often controlled manually by an experienced operator in a time-consuming process. Therefore, to accelerate the reproduction process, a tool that can help control the texture would be useful in the fields of computer graphics and imaging.

The spread of high-resolution imaging systems, such as high-definition television, is of great importance to people in the entertainment world; these people include actors, actresses, and newscasters, because their skin texture can be revealed in great detail by these imaging systems. A tool for controlling the skin appearance of entertainers would not only be useful without the real-time processing necessary for live broadcasting.

In this paper, we introduce a useful tool for skin texture control. We use the component maps of melanin, hemoglobin, and shading, which were obtained by our previous method<sup>1,2</sup>. Based on the analysis of 123 skin textures in our database, the texture of melanin is controlled continuously and physiologically. The physiological validity for the change of melanin texture is confirmed by comparing the synthesized image with an ultraviolet image, which is able to predict the change of melanin texture due to aging. The processes for the texture controls are

implemented on programmable graphics hardware, and real-time processing for a video stream is achieved by our proposed method.

In texture analysis and synthesis, numerous approaches have been proposed. Here, we briefly review some recent and representative studies which provide the background necessary for presenting our contribution. Procedural texture generation<sup>3-8</sup> is based on texture models that are helpful for specific classes of materials such as wood, marble, and animal skin. Human skin texture was never generated by this method because it is difficult to choose the control parameters of such a texture. Synthesis based on feature matching generates new images by matching the features in an example texture<sup>9-11</sup>. In this example-based approach, algorithms are classified as a parametric sampling technique. In contrast, synthesis based on neighborhoods<sup>12-20</sup> is classified as a non-parametric sampling technique in the example based approach. Recently, the synthesis based on neighborhoods has been widely accepted for practical applications due to its simplicity in implementation, speed and its ability to cover a large variety of textures. This method includes not just synthesis, but it also is expected to process the texture functionally, as in texture transfer<sup>1,16,17</sup>, texture replacement<sup>21</sup>, texture manipulation<sup>22,23</sup>, and texture control<sup>24,25</sup>. The texture transfer or replacement changes the texture from one object to another. In our previous work<sup>1</sup>, we could transfer the skin texture of a 50-year-old person into the skin texture of a 20-year-old person, although the in-between texture could not be obtained. This is because the texture generation process is not modeled in the current methods of texture transfer and replacement. In principle, texture generation methods can be applied to texture manipulation for an image by estimating the generation parameters from the image and changing them continuously during synthesis, although it is difficult to estimate the control parameters of such textures, and the generated texture is a specific class, as mentioned above. Only a few studies

have been done in the texture manipulation or control of an image, and the existing methods are limited to macrostructures<sup>22</sup> and a near-regular texture<sup>23-25</sup>. These methods cannot be applied to control human skin texture, since human skin texture is different from macrostructures and near-regular textures.

Skin textures have been analyzed and modeled in the computer vision community<sup>26,27</sup> for qualitative characterization of the skin appearance for such uses as clinical evaluation<sup>27</sup> and recognition<sup>26</sup>. The modeling of skin texture was based on three-dimensional textures<sup>28</sup>, and the texture was characterized by its response to a set of orientation and spatial frequency-selective linear filters. Leung and Malik<sup>28</sup> clustered the filter responses into a small set of prototype response vectors and used histograms of the prototype for the recognition of texture. Cula et al.<sup>26,27</sup> transformed the histogram into low-dimensional space by using principal component analysis<sup>29</sup>. Their work is very similar to our approach: in this paper, we obtain the low-dimensional space of the feature vector, which is used to control the appearance of texture. However, in addition to the difference of purpose between recognition and synthesis, it should be noted that a histogram of a prototype is not as easily controlled as a histogram of a pixel value, which is used in our paper for the histogram matching process.

In the real-time processing system for a live-video stream, numerous approaches and applications have been proposed (for example, see Open Source Computer Vision Library: OpenCV library by the Intel corporation). Debevec et al.<sup>30</sup> achieved a live-action composition between a human at a site and a stream of environmental maps. Matusik and Pfister<sup>31</sup> built a scalable system for the real-time acquisition, transmission, and display of 3D scenes. With the recent development of programmable graphics hardware, it is becoming easier to process a

real-time video stream on graphics hardware. In this paper, we used graphics hardware to accelerate the process of pyramid decomposition and composition for melanin texture.

This paper can be divided into the following three capabilities. (1) Continuous texture control of human skin: The melanin texture is decomposed into layers with different spatial frequencies based on the multi-resolution technique. A feature vector is calculated from the histograms of the layers. The feature vector obtained is continuously shifted in the principal space of the melanin texture to continuously control the appearance of the texture. (2) A data-driven physiological model of skin texture: The principal space is constructed based on the texture database to extract physiologically plausible changes of the melanin texture. Controlling the feature vector in the principal space is also based on the database, which contains pairs of the texture image and the texture attribute. (3) A real-time processing system for skin texture control: A live-video stream is processed to change the appearance of skin by the above techniques. We used programmable graphics hardware to accelerate the process of multi-resolution decomposition. To the knowledge of these authors, no previous work has achieved the above capabilities. The proposed method is expected to reduce the processes for skin appearance control and to perform real-time processing for facial video streams for various applications such as live broadcasting.

## **2. DATA-DRIVEN PHYSIOLOGICALLY BASED SKIN TEXTURE**

### **CONTROL**

We used our previous technique<sup>1, 2</sup> to separate two images with different polarizing filters into specular, shading, melanin and hemoglobin components, as shown in Figure 1. Since the original process was unstable for obtaining well-separated components, we improved the technique by introducing an interactive operation for finding the basis vector of the components.

(The process of separation will be briefly described in Section 3.) In this section, the separated skin melanin component is used to control the skin appearance. Figure 2 shows an overview of the process for controlling the skin melanin texture. The input texture is decomposed by the Laplacian pyramid method<sup>32</sup> into layers with different spatial frequencies. The histograms of the layers are analyzed, and feature vector  $\mathbf{f}$  is extracted to represent the histograms. The obtained feature vector is shifted in the principal space of the melanin texture to control the appearance of the texture. This space is constructed by 123 samples of melanin texture from our own database. Figure 3 shows part of the database used in this paper. The shifted feature vector  $\mathbf{f}'$  is inversely transformed into histograms of the layers. The pixel values at each layer of the input texture are transformed<sup>7</sup> by a lookup table created for matching the original histograms and the histograms synthesized by the shifted feature vector  $\mathbf{f}'$ . The transformed layers make up the synthesized texture. By controlling the feature vector continuously in the principal space, the texture can be animated continuously according to the data-driven, physiologically based skin texture control. The details of extracting the feature vector, constructing the principal space, and controlling the feature vector in the space are described in the following paragraphs.

The texture is decomposed into the first through fifth layers, since five layers is enough to represent the appearance of skin in our decided resolution of the image. The resolution is 6 pixels/mm for the images in our database and in the imaging system used in the section on real-time processing (Section 3). The fifth layer is a low-pass component of the texture, and this is not modeled and controlled in this paper. The first to fourth layers are modeled and controlled as follows. A normalized histogram  $h_i(v)$  is calculated for each layer. The index  $i$  is the number of the layer and  $v$  is the value of the components. Since the sum of the values in the histogram is the pixel number, the normalized histogram can be defined as Equation (1).

$$\int_{-\infty}^{+\infty} h_i(v) dv = 1 \quad (1)$$

Figure 4 shows the histogram at each layer for four examples of textures. It can be seen that the histogram in the first and second layers can be modeled by Gaussian distribution with a mean value of 0. Only the standard deviation  $\sigma_i$  of the histogram is used as the model parameter, since the histogram is normalized in Equation (1).

$$\sigma_i = \sqrt{\int_{-\infty}^{+\infty} \{h_i(v)\}^2 dv} \quad i = 1 \text{ or } 2 \quad (2)$$

We can also see that the histogram in the third and fourth layers is modeled not only by Gaussian distribution, but also by the high-density region. The high-density region is an important part for expressing the characteristic of the melanin stain. We modeled the histogram using a combination of the Gaussian distribution and exponential distribution in the high-density region. The parameter of the Gaussian distribution is extracted using only the left side of the histogram, as follows.

$$\sigma_i = \frac{1}{2r_{left}} \sqrt{2 \int_{-\infty}^0 \{h_i(v)\}^2 dv} \quad i = 3 \text{ or } 4 \quad (3)$$

$$\text{where } r_{left} = \int_{-\infty}^0 h_i(v) dv$$

We set a threshold value  $thresh\_i$  empirically to decide the characteristic high-density region ( $v > thresh\_i$ ). The high-density region is modeled by  $a_i \exp\{u_i(v - thresh\_i)\}$ , where  $a_i$  is the value of the modeled Gaussian distribution at  $v = thresh\_i$ . Let us define the function  $N(v; m, \sigma)$  as the normalized Gaussian distribution of mean value  $m$  and standard deviation  $\sigma$ . Using the residual sum

$$r_i = 1 - \int_{-\infty}^{thresh\_i} 2r_{left} N(v; 0, \sigma_i) dv \quad (4)$$

in the high-density region ( $v > thresh\_i$ ) after modeling the Gaussian distribution, the

attenuation coefficient  $u_i$  is obtained by solving the following equation.

$$\int_{thresh\_i}^{\infty} a_i \exp\{u_i(v - thresh\_i)\} dv = r_i \quad (5)$$

The modeled Gaussian distribution in the range of  $v \leq thresh\_i$  and the exponential distribution in the range of  $v > thresh\_i$  are reconstructed using  $\sigma_i$  in Equation (3) and residual sum  $r_i$  in Equation (4). Now, we have six model parameters, and we define the feature vector as  $\mathbf{f} = [\sigma_1, \sigma_2, \sigma_3, \sigma_4, r_3, r_4]^t$ , where  $[\cdot]^t$  represents transposition. The histograms of the first to fourth layers are well approximated by this feature vector to express the texture.

The principal space is necessary to control the texture in physiologically plausible changes. Therefore, the principal space is constructed based on the texture database. Figure 3 shows examples of melanin texture in the texture database. It is also necessary to consider the human sensitivity to the change of texture for each feature, since unobserved physiologically plausible changes will not mean anything to changes of the skin appearance. For this purpose, we normalized each component of the feature vector by using the degree of human sensitivity to each component. The degree of human sensitivity is alternatively obtained by using the reciprocal of the just noticeable difference (JND); thus, the normalized feature vector  $\hat{\mathbf{f}}$  is calculated as

$$\hat{\mathbf{f}} = \begin{bmatrix} 1/JND_{\sigma_1} & 0 & \cdots & 0 \\ 0 & \ddots & & \vdots \\ \vdots & & \ddots & 0 \\ 0 & \cdots & 0 & 1/JND_{r_2} \end{bmatrix} \mathbf{f} \quad (6)$$

by using the just noticeable difference  $JND_{\sigma_i}$  or  $JND_{r_i}$  for each feature. The JND value is obtained by subjective evaluation of the textures, which have a gradually changing parameter. We apply principal component analysis to the samples of normalized feature vector  $\hat{\mathbf{f}}$  in the

database to extract the physiologically plausible space of changes and obtain the first, second and third normalized principal vectors  $\mathbf{b}_1, \mathbf{b}_2, \mathbf{b}_3$  and components  $p_1, p_2, p_3$ . The components are also normalized by the square root of the eigenvalue for each sample, as follows.

$$\mathbf{p} = \Sigma^{-1} B(\hat{\mathbf{f}} - \bar{\mathbf{f}}) \quad (7)$$

where  $\mathbf{p} = [p_1, p_2, p_3]^t$ ,  $B = [\mathbf{b}_1, \mathbf{b}_2, \mathbf{b}_3]^t$ ,  $\Sigma$  is the diagonal matrix whose components are the square roots of the eigenvalues, and  $\bar{\mathbf{f}}$  is the mean vector in the samples. The contribution ratio for three components is 0.988, therefore, three components are enough to represent the change of texture.

Figures 5(a) and (b) show the distribution of the normalized principal components in the principal space. Controlling the feature vector in the principal space is based on pairs of the texture and texture attribute in the database. In this paper, yellow-unevenness  $Y$  and age  $A$  are used as attributes of the texture. These values are written below each texture image in Figure 3, and the colors of each plot in Figure 5 are related to (a) yellow-unevenness or (b) age. From red, green, blue, cyan, magenta, yellow, to black, the value of yellow-unevenness changes from 1.0 to 5.0, and age changes from teens to eighties. The values of yellow-unevenness are obtained by subjective evaluation by experts in the cosmetics development field, and are commonly used in that field. Based on the pair of normalized principal component  $\mathbf{p}_i$  and attribute  $a_i$  of the  $i$ -th sample in  $N$  samples,  $(\mathbf{p}_1, a_1), (\mathbf{p}_2, a_2), (\mathbf{p}_3, a_3), \dots, (\mathbf{p}_N, a_N)$ , the principal direction  $\boldsymbol{\rho}$  of change for that attribute is obtained by linear multiple regression analysis as follows.

$$\begin{bmatrix} \boldsymbol{\rho} \\ b \end{bmatrix} = \begin{bmatrix} P & \mathbf{1} \end{bmatrix} \left( \begin{bmatrix} P & \mathbf{1} \end{bmatrix} \begin{bmatrix} P & \mathbf{1} \end{bmatrix}^t \right)^{-1} \mathbf{a} \quad (8)$$

where  $P = [\mathbf{p}_1^t \ \dots \ \mathbf{p}_N^t]^t$ ,  $\mathbf{a} = [a_1 \ \dots \ a_N]^t$ ,  $\mathbf{1} = [1 \ \dots \ 1]^t$  and  $b$  is the bias value obtained at the same time. The principal direction  $\boldsymbol{\rho}$  is drawn in Figures 5(a) and (b) for

yellow-unevenness and age, respectively. The directions are similar to each other, and the correlation coefficients are 0.72 and 0.48 for yellow-unevenness and age, respectively. By using this principal direction, we can control the feature vector continuously in the principal space as follows.

$$\mathbf{p}' = \mathbf{p} + s\boldsymbol{\rho} \quad (9)$$

$$\hat{\mathbf{f}}' = \sum B' \mathbf{p}'_i + \bar{\mathbf{f}} \quad (10)$$

where  $s$  is the tag for controlling the skin texture.

Figure 6 shows examples of the resulting continuous syntheses for three original images with different degrees of stain. The realistic continuous change of skin texture can be seen in the series of images. Figure 7 also shows the continuous change of facial appearance by the same technique. The second image from the left is the original facial image and texture.

It is known that the skin image taken by ultraviolet (UV) light can predict the change of the skin in aging. Figures 8(a), (b), (c) show the original image, UV image, and controlled image using the above method, respectively. It can be seen that the change of texture is predicted well in the proposed method; therefore, it can be said that we can confirm the physiological validity of the proposed melanin texture control.

### 3. REAL-TIME PROCESSING SYSTEM FOR SKIN TEXTURE

Figure 9 shows the flow of the real-time processing system for the facial appearance analysis and synthesis developed in this paper. For surface reflection separation, it is necessary to use a polarized filter with polarized light. Although a computer vision technique can also be used in color vector space, we used the polarized filters to obtain the high-quality images in this paper. A beam splitter was placed between the two cameras at a 45-degree angle. The two video signals obtained through the different orientations of the polarizer are digitized into the personal computer. In the computer's CPU, the two images are processed into the specular, shading,

melanin and hemoglobin components. A mask image of the skin region is also calculated from the melanin and hemoglobin components. These operations are performed at 25 frames per second by using a  $256 \times 256 \times 256$  lookup table for the diffuse reflection image. All components are transferred into the graphics processing unit (GPU) to control the appearance by such user interface tools as a mouse and keyboard. The graphics processing unit synthesizes the controlled components into the image to be displayed on the monitor. The graphics processing unit can operate at 28 frames per second in these processes, but we get 17 frames per second for video stream processing due to the bottleneck at the connection between the CPU and GPU.

*Offline* processing is necessary to achieve the above *online* real-time processing. The CPU receives two images as input from the optical system. We define  $\mathbf{v}_{sp}$  as the color vector taken by the P polarized illumination and S polarized filter in front of the camera at the current pixel, and  $\mathbf{v}_{ss}$  is the vector taken by the P polarized illumination and P polarized filter. The diffuse reflectance components  $\mathbf{v}_d$  are calculated as  $\mathbf{v}_d = 2\mathbf{v}_{ps}$  and the secular reflectance components  $\mathbf{v}_{sp}$  are calculated as  $\mathbf{v}_{sp} = 2(\mathbf{v}_{pp} - \mathbf{v}_{ps})$ . The lookup table for the diffuse reflection to extract the components is built offline in this paper. The process of building the lookup table is as follows. The diffuse reflection is transformed into the density space as  $\mathbf{v}_d^{\log} = -\log(\mathbf{v}_d)$ . The diffuse component in the density space is separated into the component vector of the melanin, hemoglobin and shading components as follows,

$$\mathbf{c} = B^{-1}\mathbf{v}_d^{\log} \quad (11)$$

where  $B = [\mathbf{b}_M \quad \mathbf{b}_H \quad \mathbf{I}]$  and  $\mathbf{b}_M$ ,  $\mathbf{b}_H$  are the basis vectors for melanin and hemoglobin, respectively, in the density space, and  $\mathbf{I}$  is the vector for shading. The skin region is extracted from the melanin and hemoglobin components and stored as mask components. The transformation from the diffuse color  $\mathbf{v}_d$  to the shading, melanin, hemoglobin, and mask components are implemented by the  $256 \times 256 \times 256$  lookup table, and this table is used in the

real-time processing.

The basis vectors for the melanin and hemoglobin components,  $\mathbf{b}_M$  and  $\mathbf{b}_H$ , are also extracted by the offline process by using the independent components analysis, as was done in our previous method<sup>1</sup>. Because this original method occasionally fails to extract the components in our imaging system, we modified the technique by introducing a two-step interactive process. From the pattern of the texture of the components, it is easy to evaluate the separated map of components, whether they are well separated or not. The first step of the interactive technique iterates the independent components analysis by changing the region of the analysis, and then the separation is evaluated by the user. The iteration will finish if the separation is evaluated as generally valid. The second step of the interactive technique is performed interactively to adjust the basis vectors,  $\mathbf{b}_M$  and  $\mathbf{b}_H$ , to adequately separate the melanin and hemoglobin components. The adjustment is performed using the graphical user interface to move the basis vector in two-dimensional space, and the resulting separations are visualized in real time. The lookup table for histogram matching is also made offline. We prepared a continuous series of lookup tables to change the tag value  $s$  continuously in Equation (9).

In the online process of the real-time processing, the graphics hardware receives the specular, shading, melanin, hemoglobin, and mask video signals from the CPU. The melanin image is decomposed by the Laplacian pyramid, and the lookup table for histogram matching is applied at each layer and composed as a synthesized texture. The lookup tables are switched at the user interface in the application program. All processed components of vector  $\mathbf{c}'$  are combined as the modified diffuse image in the density space. The image in the density space is transformed into the image in the intensity space by using the lookup table of exponential operations.

Figure 10 shows examples of real-time processing for a human face. Figure 10(a) shows the overview of the scene, (b) shows the change of surface reflection, and (c) shows the change of the

melanin texture. We can see that an interactive change in the skin appearance is achieved in real time in the proposed system.

#### **4. CONCLUSION AND DISCUSSION**

The texture of the melanin component was controlled continuously and physiologically, based on the analysis of 123 skin textures in our database. The real-time change of the skin texture appearance was demonstrated for a video stream of the human face by using the graphics hardware. The resulting video stream showed the effectiveness of this system in realistically controlling the skin appearance for the purpose of processing live broadcasting.

In the melanin texture analysis, matching the resolution between the image in the database and the input skin image in the system is very important for obtaining a meaningful change of the melanin texture. In the practical application of live broadcasting, camera zooming should be monitored to calibrate the resolution in real time. Facial movement should also be tracked to apply stable control of the skin appearance on the face.

The amount of offline processing for finding the basis vector is a drawback of our system for practical applications. If the imaging system is decided, it is experimentally known that the basis vector will not deviate a lot in individual Asian people. Therefore, the average basis vector can be used for specific applications for specific people. The main limitation of our method in the current system is that, in all the processing in the system, it is assumed that the object consists of two-dimensional planes. Rotational movement of the face and the three-dimensional shape of the face give an error in those regions where the resolution match is broken. The proposed process should be extended to an arbitrary manifold surface<sup>33, 34</sup> for more robust processing.

The physiological principal vector is extracted by the technique of multiple regression analysis in Equation (8). The correlation coefficient of age is quite low compared to that of yellow-unevenness, since the appearance of the melanin texture is not correlated just with age. The appearance of the melanin texture is highly influenced by the differences among

individuals. By using multiple regression analysis, we managed to extract the trend of the change of appearance caused by aging with a correlation coefficient of 0.48. To improve this change of appearance, we tried to introduce higher-order terms in the multiple regressions to consider the nonlinear property of the sample subspace. However, we could not find nonlinear terms that were as effective as those of the linear subspace. To manage the differences among individuals, it is necessary to build a new skin image database by monitoring each volunteer during his or her life.

The proposed physiologically plausible change is based on a database of real skin images, not physiological processes for melanin generation. Melanin pigments are produced and stored in melanosomes. In human epidermal melanocytes, melanosomes are transported from the perinucleus to the peripheral region of the melanocytes. Currently, the process of melanin transport is being studied by Kuroda and Fukuda<sup>35</sup>, and this study is expected to reveal the generation process of melanin in the skin. We expect that our extracted features will correlate with the chemical substances in melanin generation, and the change of the melanin texture from the radiation of ultraviolet light will be predicted in a more meaningful way to simulate the realistic changes of skin appearance.

## **ACKNOWLEDGEMENTS**

We wish to thank Ryoko Usuba at Chiba University, and Mitsuhiro Shiraishi and Natsuko Okiyama at Kao Corporation for their skin texture database and valuable comments. This research is partly supported by a JSPS Grants-in-Aid for Scientific Research (16760031).

## **REFERENCES**

1. N. Tsumura, N. Ojima, K. Sato, M. Shiraishi, H. Shimizu, H. Nabeshima, S. Akazaki, K. Hori and Y. Miyake, “Image-based skin color and texture analysis/synthesis by extracting hemoglobin and melanin information in the skin,” Proceedings of ACM SIGGRAPH 2003, 770-779 (2003).
2. N. Tsumura, H. Haneishi and Y. Miyake, “Independent component analysis of skin color image,” Journal of Optical Society of America A **16**, 9, 2169-2176(1999).
3. K. Perlin, “An image synthesizer,” Proceedings of ACM SIGGRAPH 85 287–296(1985).
4. A. Witkin and M. Kass, “Reaction – diffusion textures,” Proceedings of ACM SIGGRAPH 91, 299–308(1991).
5. G. Turk, “Generating textures on arbitrary surfaces using reaction-diffusion,” Proceedings of ACM SIGGRAPH 91, 289–298(1991).
6. K. Fleischer, D. Laidlaw, B. Currin, and A. Barr, “Cellular texture generation,” Proceedings of ACM SIGGRAPH 95, 239-248 (1995).
7. S. Worley, “A cellular texture basis function,” Proceedings of ACM SIGGRAPH 96, 291–294(1996).

8. M. Walter and A. Fournier, "Clonal mosaic model for the synthesis of mammalian coat patterns," *Graphics Interface '98*, 82–91(1998).
9. D. J. Heeger and J. Bergen, "Pyramid-based texture analysis/synthesis," *Proceedings of ACM SIGGRAPH 95*, 229-238(1995).
10. J. De Bonet, "Multiresolution sampling procedure for analysis and synthesis of texture images," *Proceedings of ACM SIGGRAPH 97*, 361-368(1997).
11. E. Simoncelli and J. Portilla, "Texture characterization via joint statistics of wavelet coefficient magnitudes," *Proc. of Fifth International Conference on Image Processing*, **1**, 62–66(1998).
12. A. Efros and T. Leung, "Texture synthesis by non-parametric sampling," *Proc. of Intl. Conf. Computer Vision*, 1033-1038(1999).
13. L.-Y. Wei and M. Levoy, "Fast texture synthesis using tree-structured vector quantization," *Proceedings of ACM SIGGRAPH 2000*, 479–488(2000).
14. M. Ashikhmin, Synthesizing natural textures. In *ACM Symposium on Interactive 3D Graphics*, 217-226(2001).

15. L. Liang, C. Liu, Y. Xu, B. Guo and H.-Y. Shum, "Real-time texture synthesis using patch-based sampling," *ACM Trans. Graphics* **20**, 3, 127-150(2001).
16. A. Hertzmann, C. Jacobs, N. Oliver, B. Curless and D. Salesin, "Image analogies," *Proceedings of ACM SIGGRAPH'01*, 327-340(2001).
17. A. Efros and W. Freeman, "Image quilting for texture synthesis and transfer," *Proceedings of ACM SIGGRAPH'01*, 341-346(2001).
18. J. Zhang, K. Zhou, L. Velho, B. Guo and H. SHUM, "Synthesis of progressively-variant textures on arbitrary surfaces," *Proceedings of ACM SIGGRAPH 2003*, 295-302(2003).
19. V. Kwatra, A. Schodl, I. Essa, G. Turk and A. Bobick, "Graphcut textures: Image and video synthesis using graph cuts," *Proceedings of ACM SIGGRAPH'03*, 277-286(2003).
20. Q. Wu and Y. Yu, "Feature Matching and Deformation for Texture Synthesis," *Proceedings of ACM SIGGRAPH 2004*, 364-367(2004).
21. Y. Tsin, Y. Liu and V. Ramesh, "Texture replacement in real images," *Proc. of IEEE Computer Vision and Pattern Recognition Conference*, 539-544(2001)

22. J.-M. Dischler and D. Ghazanfarpour, "Interactive image-based modeling of macrostructured textures," *IEEE Computer Graphics and Applications* **19**, 1, 66–74(1999).
23. Y. Liu and W. Lin, "Deformable texture: the irregular regular-irregular cycle," *Proc. of The 3rd International Workshop on Texture Analysis and Synthesis*, 65-70(2003).
24. S. Lefebvre, H. Hoppe, "Parallel controllable texture synthesis," *Proceedings of ACM SIGGRAPH 2005*, 787-794 (2005).
25. W. Matusik, M. Zwicker F. Durand , "Texture Design Using a Simplicial Complex of Morphable Textures," *Proceedings of ACM SIGGRAPH 2005*, 777-786(2005)
26. O. G. Cula and K. J. Dana, "3D texture recognition using bidirectional feature histograms," *International Journal of Computer Vision*, **59**, 1, 33–60(2004)
27. O. G. Cula and K. J. Dana , F.P. Murphy, B.K. Rao, "Bidirectional imaging and modeling of skin texture," *IEEE Transactions on Biomedical Engineering*, **51**, 12, 2148- 2159(2004).
28. T. Leung and J. Malik, "Representing and recognizing the visual appearance of materials using three dimensional textures," *International Journal of Computer Vision*, **43**, 1, 29–44(2001).

29. W. Matusik, H. Pfister, M. Brand, L. McMillan, A Data-Driven Reflectance Model, Proceedings of ACM SIGGRAPH 2003, 759-769(2003)
30. P. Debevec, T. Hawkins, C. Tchou, H.-P. Duiker, W. Sarokin and M. Sagar, “Acquiring the reflectance field of a human face,” Proceedings of ACM SIGGRAPH 2000, 145-156(2000).
31. W. Matusik and H. Pfister, “3D TV: A Scalable System for Real-Time Acquisition, Transmission, and Autostereoscopic Display of Dynamic Scenes,” Proceedings of ACM SIGGRAPH'04, 811-824(2004).
32. P. J. Burt and E. H. Adelson, “A multiresolution spline with application to image mosaics,” ACM Transactions on Graphics, **2**, 4, 217–236(1983).
33. G. Turk, “Texture Synthesis on Surfaces,” Proceedings of ACM SIGGRAPH 2001 347–354(2001).
34. L.-Y. Wei and M. Levoy, “Texture Synthesis over Arbitrary Manifold Surfaces,” Proceedings of ACM SIGGRAPH 2001 355–360(2001).
35. T. S. Kuroda and M. Fukuda, “Rab27A-binding protein Slp2-a is required for peripheral melanosome distribution and elongated cell shape in melanocytes,” Nature Cell Biology **6**, 1195 – 1203(1994).

## Figure Captions

Figure 1. Separation of two images with different polarizing filters into specular, shading, melanin, and hemoglobin components based on our previous method. In this paper, interactive separation is introduced into the original method to improve the separated results.

Figure 2. Process of controlling the skin melanin texture proposed in this paper.

Figure 3. Skin melanin texture database (18 of 123 samples). The values written below each texture image are Yellow-unevenness  $A$  and age  $Y$ .

Figure 4. Various types of skin melanin textures and their histograms in the layers of the Laplacian pyramid decomposition.

Figure 5. Plots in the principal space of 123 skin melanin textures, and the control direction for aging and yellow-unevenness. The colors of each plot are related to the (a) yellow-unevenness or (b) age. The arrows indicate the principal direction of change.

Figure 6. Results of the skin appearance change for three original images by the data-driven, physiologically based melanin texture control.

Figure 7. The continuous melanin texture controls based on the data-driven physiological model from the skin texture database. The second image from the left is the original facial image and texture.

Figure 8. Comparing the synthesized image with the UV image, which is able to predict the change of melanin texture in aging. (a) shows the original image, (b) the UV image, and (c) the controlled image.

Figure 9. Flow of the real-time processing system for the facial appearance analysis and continuous synthesis developed in this paper.

Figure 10. The real-time processing by the developed system. (a) shows the overview of the scene, (b) the change of surface reflection, (c) the change of the melanin texture.

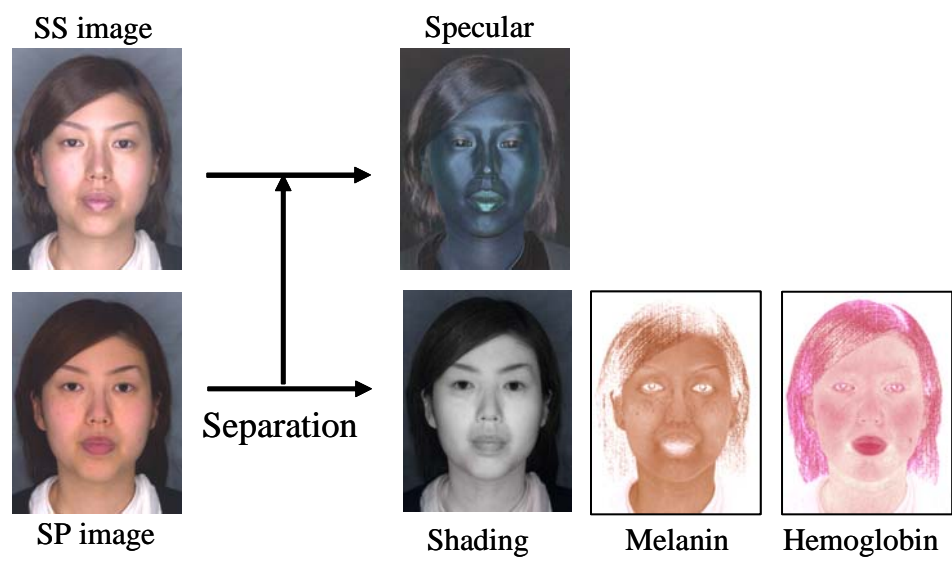


Fig. 1. Separation of two images with different polarizing filters into specular, shading, melanin, and hemoglobin components based on our previous method. In this paper, interactive separation is introduced into the original method to improve the separated results.

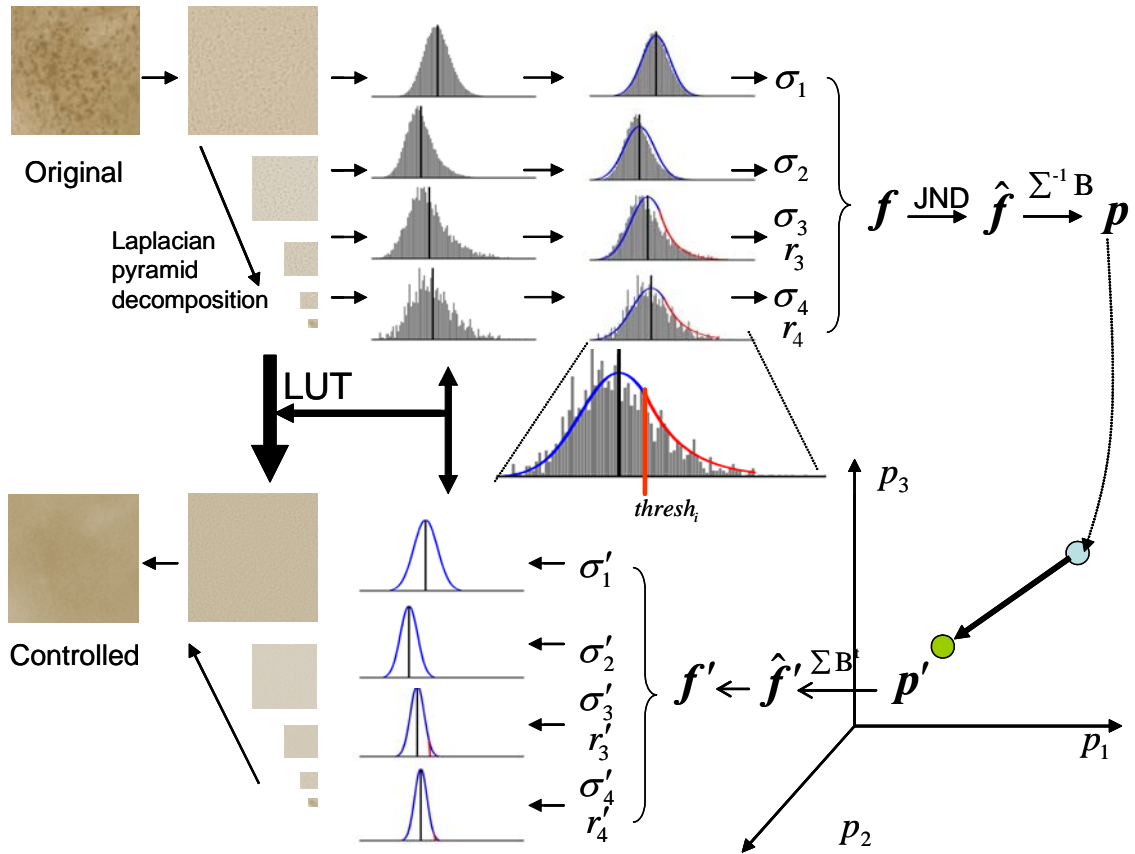


Fig. 2. Process of controlling the skin melanin texture proposed in this paper.

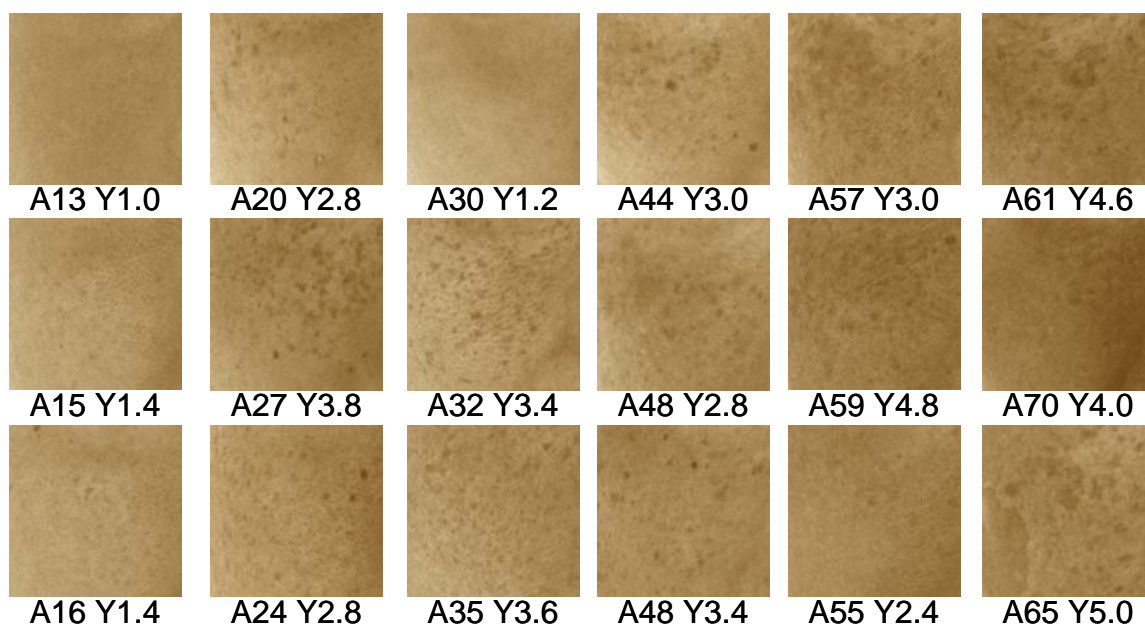


Fig. 3. Skin melanin texture database (18 of 123 samples). The values written below each texture image are Yellow-unevenness A and age Y.

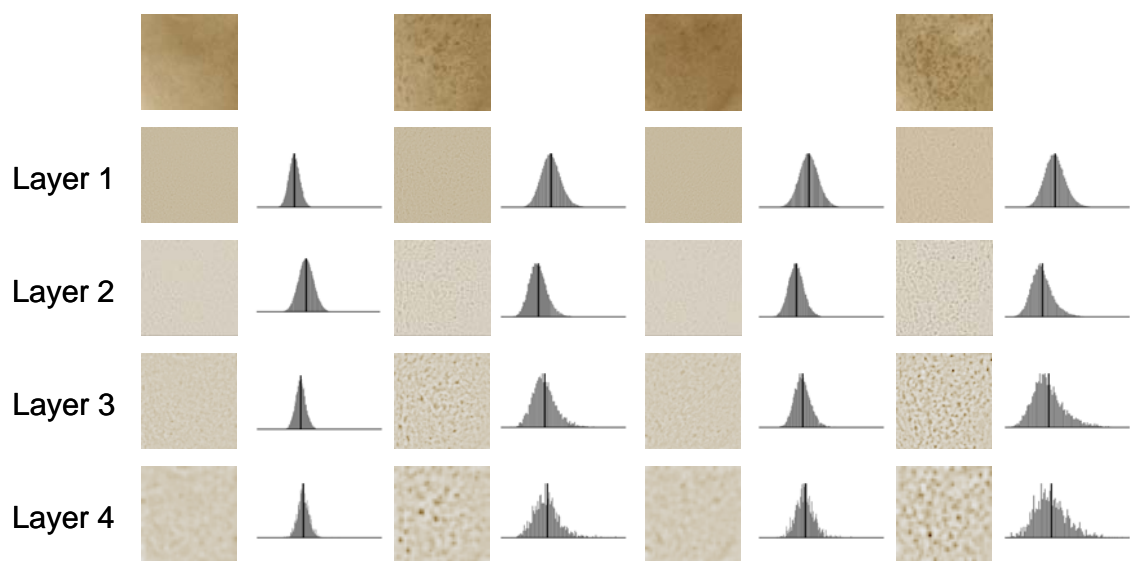


Fig. 4. Various types of skin melanin textures and their histograms in the layers of the Laplacian pyramid decomposition.

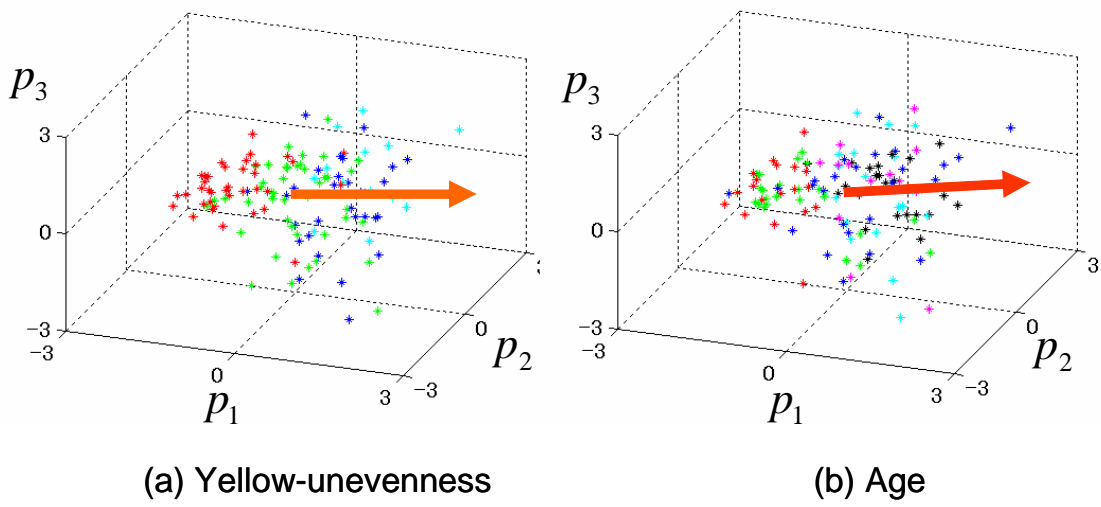


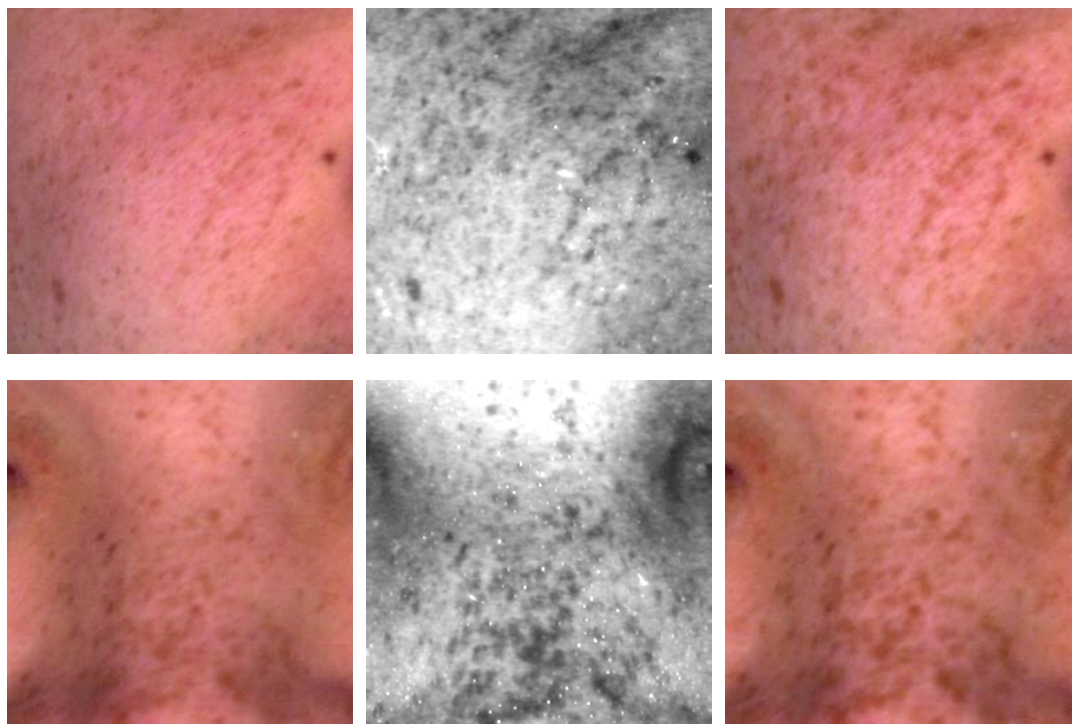
Fig. 5. Plots in the principal space of 123 skin melanin textures, and the control direction for aging and yellow-unevenness. The colors of each plot are related to the (a) yellow-unevenness or (b) age. The arrows indicate the principal direction of change.



Fig. 6. Results of the skin appearance change for three original images by the data-driven physiologically based melanin texture control.



Fig. 7. The continuous melanin texture controls based on the data-driven physiological model from the skin texture database. The second image from the left is the original facial image and texture



(a) Original image      (b) UV image      (c) Synthesized image

Fig. 8. Comparing the synthesized image with the UV image, which is able to predict the change of melanin texture in aging. (a) shows the original image, (b) the UV image, and (c) the controlled image.

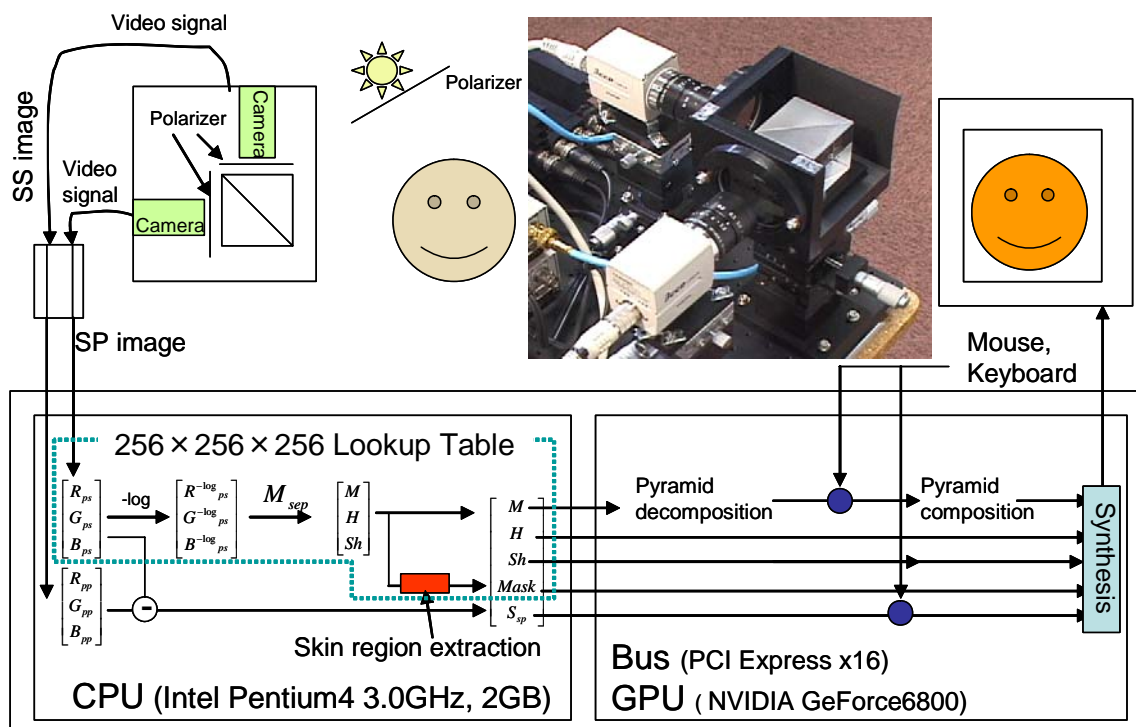


Fig. 9. Flow of the real-time processing system for the facial appearance analysis and continuous synthesis developed in this paper.



(c) Change of texture: (Left) original, (Right) synthesis



(a) Overview



(b) Change of surface reflection

Fig.10. The real-time processing by the developed system. (a) shows the overview of the scene, (b) the change of surface reflection, (c) the change of the melanin texture.